



HAL
open science

Influence of the Arctic Sea-Ice Regime Shift on Sea-Ice Methylated Mercury Trends

Amina Schartup, Anne Soerensen, Lars-Eric Heimbürger-Boavida

► **To cite this version:**

Amina Schartup, Anne Soerensen, Lars-Eric Heimbürger-Boavida. Influence of the Arctic Sea-Ice Regime Shift on Sea-Ice Methylated Mercury Trends. *Environmental Science and Technology Letters*, 2020, 10.1021/acs.estlett.0c00465 . hal-02935234

HAL Id: hal-02935234

<https://hal.science/hal-02935234>

Submitted on 13 Nov 2020

HAL is a multi-disciplinary open access archive for the deposit and dissemination of scientific research documents, whether they are published or not. The documents may come from teaching and research institutions in France or abroad, or from public or private research centers.

L'archive ouverte pluridisciplinaire **HAL**, est destinée au dépôt et à la diffusion de documents scientifiques de niveau recherche, publiés ou non, émanant des établissements d'enseignement et de recherche français ou étrangers, des laboratoires publics ou privés.

1 **Influence of Arctic Sea-Ice Regime Shift on Sea-Ice Methylated Mercury**
2 **Trends**

3
4 Amina T. Schartup,¹ Anne L. Soerensen² and Lars-Eric Heimbürger-Boavida³

5
6 ¹Scripps Institution of Oceanography, La Jolla CA, USA

7 ²Swedish Museum of Natural History, Department of Environmental Research and Monitoring,
8 Stockholm, Sweden

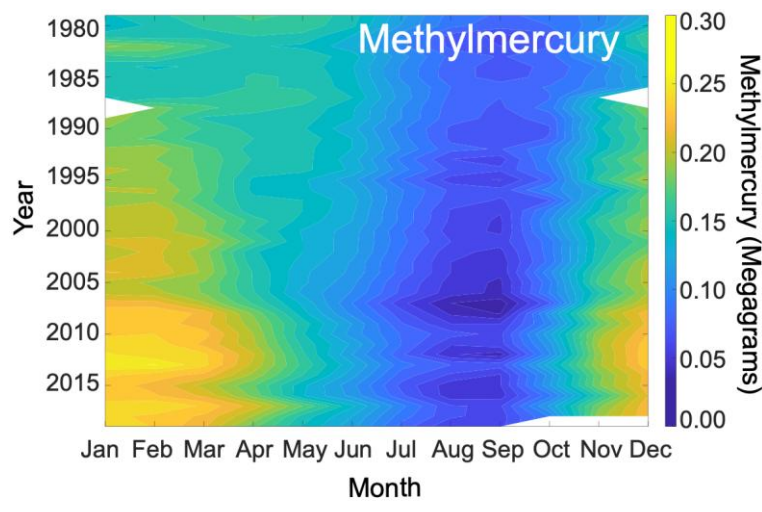
9 ³Aix Marseille Université, CNRS/INSU, Mediterranean Institute of Oceanography (MIO) UM
10 110, Marseille, France

11
12
13 Correspondence to: aschartup@ucsd.edu
14

15
16 **Abstract**

17 Arctic sea-ice regulates the air-sea exchange of volatile mercury (Hg) species like
18 dimethylmercury (DMHg) or elemental Hg, and is known to host Hg methylating microbes that
19 produce neurotoxic and biomagnifying monomethylmercury (MMHg). Arctic sea-ice accounts
20 for 57% of the total primary production in the Arctic Ocean suggesting that it could be the main
21 source of MMHg to arctic food-webs. Despite this, little is known about Hg concentrations and
22 speciation in arctic sea-ice. Here, we report Hg species and show the importance of sea ice
23 composition on sea-ice methylmercury (MeHg = DMHg+MMHg) budgets. We propose that the
24 shift from older sea-ice (lower MeHg) to younger sea-ice (higher MeHg) resulted in a 40%
25 increase in MeHg (per m² of sea-ice) since 1979 despite a 45% decline in the total sea-ice

26 volume. About 30% of the MeHg sea-ice budget is DMHg, this means that when the sea-ice
27 melts in the summer it could contribute $0.03 - 2.7 \text{ pmol m}^{-2} \text{ day}^{-1}$ of DMHg to the atmosphere
28 which is comparable to diffusion from water ($0.48 - 2.8 \text{ pmol m}^{-2} \text{ day}^{-1}$). This study shows that
29 the MeHg content of rapidly shrinking arctic sea-ice and exposure of sea-ice biota may not be
30 declining as previously thought.



31

32

33

34 **TOC abstract**

35

36 **Keywords:** Dimethylmercury, monomethylmercury, climate change, GEOTRACES

37

38

39

40

41

42

43

44

45 **Introduction**

46 The Arctic Ocean's unique physical characteristics and food-web structure influence the
47 biogeochemical cycle of neurotoxic monomethylmercury (MMHg), allowing it to reach high
48 levels in arctic biota.^{1,2} In the Arctic, MMHg is a health concern for marine wildlife and human
49 communities dependent on arctic ecosystems for hunting and fishing.^{1,3} Among the physical
50 characteristics, the presence of sea-ice has been identified as a possible explanation for the
51 higher production and biomagnification of MMHg observed in the Arctic Ocean.² Sea-ice
52 regulates air-sea exchange of volatile Hg species (elemental Hg-Hg⁰ and dimethylmercury -
53 DMHg) by capping the water column and letting Hg build up under the ice.^{4,5} The mechanism of
54 sea-ice production and melting creates a highly stratified surface water column that has been
55 proposed to enhance MMHg production.⁶⁻⁸ Sea-ice can also impact MMHg exposure through
56 biologically mediated MeHg production within the sea-ice itself, as suggested by Beattie *et al.*⁹
57 based on a study of total methylated Hg species (MeHg = MMHg + DMHg) in two arctic sea-ice
58 cores. Several studies showed a positive correlation between chlorophyll a (a proxy for primary
59 production) and MeHg concentration in arctic and antarctic sea-ice, suggesting that MeHg is
60 biologically produced.⁹⁻¹¹ Recently, Gionfriddo *et al.*¹¹ further identified putative Hg
61 methylating bacteria (*Nitrospina*) in antarctic first-year ice (FYI) and arctic frost flowers, but the
62 mechanism of Hg methylation in sea ice remains unknown. Compared to other arctic MMHg
63 reservoirs the total amount of MMHg stored in sea-ice is small,¹² but arctic sea-ice algae and
64 sub-ice phytoplankton account for 57% of the total annual primary production in the Arctic
65 Ocean.^{13,14} This implies that MMHg produced in the sea-ice and bioaccumulated by sea-ice
66 algae, may contribute disproportionately to arctic biota MMHg exposure. Since 1958, the average

67 sea-ice thickness has declined by over 60% (more than 2 m).¹⁵ Between 2002 and 2017, the
68 Arctic has lost more than 50% of its oldest multi-year ice (MYI),¹⁵ and is undergoing a regime
69 shift from a system dominated by MYI (until 2011) to a system dominated by seasonal ice (FYI).
70 Despite these concerns, relatively few studies have reported concentrations of Hg and MeHg in
71 sea-ice.^{5,9,16} To address this gap, we collected 6 ice cores (2 MYI and 4 FYI), brine, frost
72 flowers, under-ice water, and melt pond water and ice during the 2015 German GEOTRACES
73 expedition (GN04). We measured total Hg and MeHg in all the samples and MMHg and DMHg
74 in 3 of the cores. To extend the spatial coverage of this study we combine our data with sea-ice
75 total Hg and MeHg samples from 5 additional locations collected in 2015 during the U.S.
76 GEOTRACES expedition (GN01).⁵

77

78 **Methods**

79 Six cores were collected between Aug 25 and Sept 22 during the 2015 GEOTRACES expedition
80 (Figure 1A, Figure S1). At each site, a Kovacs 9 cm diameter corer (Kovacs Enterprise,
81 Roseburg, USA) was used. Once retrieved, the cores were sectioned into 10 cm slices, cleaned
82 with a ceramic knife and transferred into clean plastic bags. The slices were thawed and
83 transferred into trace metal clean bottles (Nalgene FEP Teflon) while still very cold to minimize
84 loss of volatile Hg. All samples were acidified to 0.4 % v:v with double-distilled hydrochloric
85 acid. Temperature and salinity of each slice were measured during and shortly after collection,
86 respectively (Figure S2). Two of the 6 cores were identified as MYI (Cores 2 and 5) on site.¹⁷
87 We also measured total Hg and MeHg in 1 brine, 1 frost flower, 7 under ice seawater, 5 melt
88 pond water, 2 melt pond ice, and 3 snow samples (Table S2). All samples were shipped and
89 analyzed for total Hg and MeHg at Harvard University in May 2016 (Figure S3 and S4). We

90 followed well-established analytical procedures for low level total Hg and MeHg
91 measurements.^{18–20} Detailed methods and nutrient profiles are provided in the Supporting
92 Information (Figure S5). MMHg was measured on samples from which DMHg had been
93 removed by purging onboard prior to acidification. DMHg was calculated as the difference
94 between MeHg and MMHg,^{21,22} and inorganic Hg (Hg^{II}) as the difference between total Hg and
95 MeHg (Figure S3). Table 1 summarizes the Hg speciation and ancillary data in the collected sea-
96 ice cores. We calculated the brine volume according to Cox & Weeks.²³
97
98 To estimate the impact of the shift from MYI dominated to FYI dominated sea-ice on MeHg, we
99 obtained monthly sea-ice volumes and total sea area trends from 1979 to 2019 from the U.S.
100 National Snow and Ice Data Center.²⁴ We use this information and the empirical relationship
101 between sea-ice volume and MYI area reported by Kwok¹⁵ to estimate respective contributions
102 of FYI and MYI to the sea-ice volume and to the sea-ice MeHg budgets from 1979 to 2019.
103 Total Hg concentrations measured in sea-ice cores in this study, 2.72 ± 2.31 pM ($n = 78$), are not
104 statistically different (1-way ANOVA, $p = 0.92$, $n = 126$) from concentrations reported by
105 DiMento *et al.*,⁵ 2.54 ± 1.46 pM ($n = 44$; Figure S6). To increase the spatial coverage of this
106 study, we include the DiMento *et al.*⁵ sea-ice data in subsequent calculations. For continuity, we
107 rename their cores 7-11 (Figure 1A). The cores in DiMento *et al.*⁵ were not identified as FYI or
108 MYI (Table S1), thus we rely on the sea-ice thickness reported for the coring sites in Marsay *et*
109 *al.*¹⁶ and the relationship between sea-ice thickness and age²⁵ to differentiate the cores (FYI:
110 Core 7, 9; MYI: Cores 8, 10 and 11). All statistical analyses are done in MATLAB (Mathworks,
111 version R2019b).
112

113 Results and Discussion

114

115 Total Hg varies within cores, with concentrations typically higher near the surface that decline
116 sharply with core depth (Figure 1B; Figure S3). For example, in Core 4, concentrations span
117 from 0.96 to 16.1 pM. Total Hg concentrations in brine, melt ponds water and ice, under ice
118 water and snow fall within the ranges measured in the sea-ice cores and range from 2.6 pM in
119 snow to 17.3 pM in brine (SI Table S2). There is no statistical difference (1-way ANOVA, $p =$
120 0.34 , $n = 110$) between total Hg concentrations in FYI (3.00 ± 2.56 pM, $n = 57$) and MYI cores
121 (2.57 ± 2.16 pM, $n = 53$).

122

123 Similar to total Hg, MeHg varies within each core (Figure S4). For example, MeHg
124 concentrations in Core 3 range from 0.024 to 0.293 pM (Figure 1C). But the location of peaks is
125 not always at the surface, MeHg peaks are also seen at depth in FYI cores (Core 4, Figure 1C).
126 MeHg levels in brine, melt ponds water and ice, under ice water and snow also fall within ranges
127 measured in the sea-ice cores, from 0.05 pM in snow to 0.19 pM in brine (Table S2). MeHg
128 concentrations in MYI (0.026 ± 0.018 pM, $n = 52$) cores are lower (1-way ANOVA, $p < 0.01$, n
129 $= 109$) than in FYI cores (0.102 ± 0.071 pM, $n = 57$). Since the total Hg (and Hg^{II})
130 concentrations in FYI and MYI cores are not significantly different, %MeHg is lower in MYI
131 than FYI cores. Since Hg^{II} concentrations are similar in both types of cores, the difference in
132 MeHg is probably not due to Hg^{II} limitation, but may instead be due to biological or chemical
133 differences between the two types of sea-ice cores that affect *in situ* production or degradation of
134 MeHg from Hg^{II} .^{11,26,27}

135

136 Methylmercury peaks in FYI Cores 3 and 4 seem to be dictated by peaks in DMHg rather than
137 MMHg (Figure 1C). On average DMHg is 34% of MeHg in the 3 cores where DMHg and
138 MMHg were determined, but peaks at >90% at 120 cm in Core 4 (Figure 1C). The distribution of
139 DMHg within cores is consistent with physically driven processes of bubble nucleation and
140 migration observed for inert gases such as argon in FYI.^{11,28} Since very little field data exists on
141 trace gas bubble formation and diffusion through the sea-ice, modeling approaches have been
142 used to test different hypotheses. Moreau *et al.*²⁹ showed that upward moving argon gas bubbles
143 explain the change in argon profiles from a bottom peak found in “Early Spring” to a surface
144 peak found in “Late Spring”. They explain the migration by the melting of the sea-ice allowing
145 brine channels to form (increasing the brine volume) and bubbles to rise. This is consistent with
146 our data where Core 3 has a lower brine volume (4.3%) than Core 4 (5.1%, Figure S7). Core 3’s
147 DMHg profile aligns well with the “Early Spring” scenario while DMHg in Core 4 follows the
148 “Late Spring” scenario in Moreau *et al.*,²⁹ indicating that DMHg is at different stages of evasion.
149

150 We compare potential DMHg release from sea-ice to air with its diffusion from water column to
151 air. Assuming that DMHg behaves similarly to argon, as described by Moreau *et al.*,²⁹ it builds
152 up in the sea-ice during the winter months (January through May/June) and is released to the
153 atmosphere in the spring when sea-ice starts melting.³⁰ We calculate that approximately 75 km³
154 day⁻¹ of FYI are lost due to sea-ice melt between peak and low volume in 2015 (120 days). If
155 DMHg concentrations are uniform across all the cores (0.030 pM on average, ranging from
156 0.003 – 0.32 pM), 2.3 mol day⁻¹ of DMHg (0.23- 24 mol day⁻¹) are released from the sea-ice
157 during the melt season. Thus, melting sea-ice could release 0.25 pmol m⁻² day⁻¹ of DMHg over
158 the sea-ice area in 2015 to the marine boundary layer (ranging from 0.03 - 2.7 pmol m⁻² day⁻¹).

159 This is a conservative estimate since sea-ice only needs to reach a threshold porosity level (5-
160 7%), not completely melt, to start releasing DMHg, and some DMHg may have already been lost
161 prior to our sampling.²⁹ To compare the sea-ice DMHg release to diffusion from the water
162 column, we calculate diffusion using a surface water DMHg (1 m; 2015 U.S. GEOTRACES)
163 concentrations from Agather *et al.*³¹ most of which were below their detection limit of 0.012 pM,
164 atmospheric DMHg concentrations measured by Baya *et al.*⁴ for 30% ice cover (0.037 pmol m⁻³),
165 and wind speed from Lesins *et al.*³² (3 m s⁻¹ at 10.4 m). We obtain a diffusion rate from the water
166 column ranging from 0.48 to 2.8 pmol m⁻² day⁻¹ depending on the relationship between gas
167 exchange and wind speed used.³³⁻³⁵ This flux is in the same range as our conservative estimate
168 on DMHg degassing from melting sea-ice, which suggests two major impacts on the Arctic
169 Ocean Hg cycle. 1) It shows that sea-ice is an important source of DMHg to the arctic
170 atmosphere, and 2) that the early spring release of DMHg to the atmosphere from melting sea-ice
171 could reduce the concentration gradient between water and air thereby dampening the DMHg
172 diffusion from the water column.

173

174 MeHg levels in FYI cores (0.102 ± 0.071 pM, $n = 57$) are about 4 times greater than in MYI
175 cores (0.026 ± 0.018 pM, $n = 52$). Therefore, we hypothesize that all things kept equal a shift
176 from MYI to FYI could significantly impact the sea-ice MeHg budget and average
177 concentrations which could lead to higher sea-ice biota exposure.^{1,36} To test this, we calculate the
178 temporal variability of the MeHg budget considering the impact of the shifts in FYI and MYI.
179 The purpose of this calculation is to evaluate whether the magnitude of the shift alone, while all
180 other parameters are kept constant, could result in a different overall trend in the sea-ice MeHg
181 budget. We do not consider other potential changes that may dampen or exacerbate MeHg

182 concentrations in sea-ice, nor do we attempt to simulate past MeHg concentrations. Figure 2 A
183 and B illustrate the importance of considering MeHg concentrations in different sea-ice types. In
184 Figure 2A, we applied the average MeHg concentration to the total volume of sea-ice. We find
185 that the average sea-ice budget over the 41-year period is 0.33 Mg (ranging from 0.04 Mg for
186 minimum MeHg and sea-ice volume year, to 1.0 Mg for maximum MeHg and sea-ice volume
187 year). This is consistent with previously reported reservoir sizes of 0.3-2.6 Mg that were based
188 on two sea-ice cores collected in the Beaufort Sea and M'Clure Strait.^{9,12} This approach results in
189 a MeHg decline of 5.2 kg year⁻¹ mirroring the overall decline in sea-ice volume. However, if we
190 instead account for the regime shift from MYI to FYI and the different MeHg concentrations in
191 two ice types over the same time period, we arrive at a sea-ice reservoir of 0.16 Mg (ranging
192 from 0.07 to 0.31 Mg). But more importantly, we do not see a declining MeHg trend despite the
193 45% sea-ice volume decline, instead we see a slight increase in MeHg of 1.3 kg year⁻¹. The
194 September trend (minimum sea-ice cover; bottom of the shaded blue area in Figure 2B) is
195 declining 0.5 kg year⁻¹ because of the large decline in total sea-ice volume. The high bound in
196 February (maximum sea-ice cover) is increasing 3.3 kg year⁻¹ driven by the FYI increase over
197 time. The change in the MeHg mass budget corresponds to an increase in mass of MeHg per area
198 of sea-ice from 15 ng m⁻² in the 1980s to 21 ng m⁻² in the 2010s (orange line on Figure 2B). This
199 suggests a 40% increase in the exposure of sea-ice biota and underlines the importance of
200 understanding MeHg biogeochemistry in different types of sea-ice.

201

202 This study shows that sea-ice plays a role in Hg biogeochemistry that extends beyond “just a
203 cap” on water column processes. We find that FYI contains more MeHg (and DMHg) than MYI
204 and calculate that the ongoing shift from a MYI to FYI dominated Arctic Ocean may cancel out

205 the previously expected decline in MeHg contributions from sea-ice. This finding as well as the
206 shortened window between sea-ice melt and peak plankton activity,^{37,38} may have consequences
207 for the exposure of biota that relies on sea-ice for food and habitat. We also measured relatively
208 large amounts of DMHg in FYI cores, sometimes reaching >90% of MeHg. A DMHg peak was
209 for example found near the bottom of a core where sea-ice algae such as *Melosira arctica* was
210 present. DMHg could passively diffuse through gills of animals feeding on sea-ice algae³⁹ and
211 the implications of DMHg in sea-ice highlighted in this study needs further investigation.

212

213

214 **Acknowledgements:**

215 We thank the chief scientist Ursula Schauer, the German GEOTRACES lead scientist Michiel
216 Rutgers van der Loeff, and the sea-ice sampling team Gerhard Dieckmann, Ellen Damm,
217 Christiane Uhlig, Aridane Gonzales Gonzales and Andreas Krell. We also thank Captain
218 Schwarze and the crew of the research icebreaker Polarstern. ATS thanks Elsie Sunderland for
219 years of support and exceptional mentorship and for access to her analytical lab at the Harvard
220 School of Engineering and Applied Science where the reported mercury measurements were
221 performed. ATS thanks Prentiss Balcom for assistance in the lab. LEHB thanks Jeroen Sonke
222 from Geosciences Environment Toulouse for his support and guidance during his postdoc and
223 partial support from the European Research Council (ERC-2010-StG_20091028) to Jeroen
224 Sonke. LEHB also received support from AXA Research Fund and the CNRS Chantier Arctique
225 Français funding via the Pollution in the Arctic System project.

226

227 **Figure 1:** Mercury concentrations and speciation in arctic sea-ice. Panel (A) is a map showing

228 the location of sea-ice cores in dark blue (1-6) collected for this study during the 2015 German
229 GEOTRACES cruise, GN04 carried out on board of the research icebreaker Polarstern (PS94,
230 ARK XXIX/3, TransArc-II), and in light blue (7-11) published in DiMento *et al.*⁵ and collected
231 during the 2015 U.S. GEOTRACES expedition (GN01). The sea-ice extent is an August 16th,
232 2015 Multisensor Analyzed Sea Ice Extent data product, US National Snow and Ice Data Center.
233 Panel (B) shows total mercury (total Hg) profiles of Cores 3 and 4. Panel (C) shows
234 monomethylmercury (MMHg), dimethylmercury (DMHg) and total methylated mercury (MeHg)
235 distribution in Cores 3 and 4.

236

237 **Figure 2:** Sea-ice methylmercury (MeHg) budgets calculated from 1979 to 2019. **A.** Trend
238 when differences in MeHg levels in multi-year and first-year ice are not considered. The shaded
239 area captures the lowest (September) and highest (February) bounds of the sea ice MeHg
240 budgets. **B.** The MeHg total mass budget, considering different contributions from multi-year
241 and first-year sea-ice, is illustrated by the blue line. The blue shaded area captures the lowest
242 (September) and highest (February) bounds of the sea-ice MeHg budgets. The MeHg mass per
243 unit of sea-ice area is the orange line.

244

245 **References**

- 246 (1) AMAP. *Arctic Monitoring and Assessment Program 2011: Mercury in the Arctic*; 2011.
247 <https://doi.org/10.1017/CBO9781107415324.004>.
- 248 (2) Zhang, Y.; Soerensen, A. L.; Schartup, A. T.; Sunderland, E. M. A Global Model for
249 Methylmercury Formation and Uptake at the Base of Marine Food Webs. *Global*
250 *Biogeochem. Cycles* **2020**, *34* (2). <https://doi.org/10.1029/2019GB006348>.
- 251 (3) Calder, R. S. D.; Bromage, S.; Sunderland, E. M. Risk Tradeoffs Associated with
252 Traditional Food Advisories for Labrador Inuit. *Environ. Res.* **2019**, No. September, 496–
253 506. <https://doi.org/10.1016/j.envres.2018.09.005>.
- 254 (4) Baya, P. A.; Gosselin, M.; Lehnerr, I.; Louis, V. L. S.; Hintelmann, H. Determination of
255 Monomethylmercury and Dimethylmercury in the Arctic Marine Boundary Layer. **2015**,
256 1–19.
- 257 (5) DiMento, B. P.; Mason, R. P.; Brooks, S.; Moore, C. The Impact of Sea Ice on the Air-Sea
258 Exchange of Mercury in the Arctic Ocean. *Deep. Res. Part I Oceanogr. Res. Pap.* **2019**,
259 *144* (October 2018), 28–38. <https://doi.org/10.1016/j.dsr.2018.12.001>.
- 260 (6) Wang, F.; Macdonald, R. W.; Armstrong, D. a; Stern, G. a. Total and Methylated Mercury
261 in the Beaufort Sea: The Role of Local and Recent Organic Remineralization. *Environ.*
262 *Sci. Technol.* **2012**, *46* (21), 11821–11828. <https://doi.org/10.1021/es302882d>.
- 263 (7) Heimbürger, L.; Sonke, J. E.; Cossa, D.; Point, D.; Lagane, C.; Laffont, L.; Galfond, B.
264 T.; Nicolaus, M.; Rabe, B.; van der Loeff, M. R.; et al. Shallow Methylmercury
265 Production in the Marginal Sea Ice Zone of the Central Arctic Ocean. *Sci. Rep.* **2015**, *5*,
266 10318. <https://doi.org/10.1038/srep10318>.
- 267 (8) Schartup, A. T.; Balcom, P. H.; Soerensen, A. L.; Gosnell, K. J.; Calder, R. S. D.; Mason,

- 268 R. P.; Sunderland, E. M. Freshwater Discharges Drive High Levels of Methylmercury in
269 Arctic Marine Biota. *Proc. Natl. Acad. Sci.* **2015**, *112* (38), 11789–11794.
270 <https://doi.org/10.1073/pnas.1505541112>.
- 271 (9) Beattie, S. A.; Armstrong, D.; Chaulk, A.; Comte, J.; Gosselin, M.; Wang, F. Total and
272 Methylated Mercury in Arctic Multiyear Sea Ice. *Environ. Sci. Technol.* **2014**, *48* (10),
273 5575–5582. <https://doi.org/10.1021/es5008033>.
- 274 (10) Cossa, D.; Heimbürger, L.-E.; Lannuzel, D.; Rintoul, S. R.; Butler, E. C. V.; Bowie, A. R.;
275 Averty, B.; Watson, R. J.; Remenyi, T. Mercury in the Southern Ocean. *Geochim.*
276 *Cosmochim. Acta* **2011**, *75* (14), 4037–4052. <https://doi.org/10.1016/j.gca.2011.05.001>.
- 277 (11) Gionfriddo, C. M.; Tate, M. T.; Wick, R. R.; Schultz, M. B.; Zemla, A.; Thelen, M. P.;
278 Schofield, R.; Krabbenhoft, D. P.; Holt, K. E.; Moreau, J. W.; et al. Microbial Mercury
279 Methylation in Antarctic Sea Ice. *Nat. Microbiol.* **2016**, *1* (August), 16127.
280 <https://doi.org/10.1038/nmicrobiol.2016.127>.
- 281 (12) Soerensen, A. L.; Jacob, D. J.; Schartup, A. T.; Fisher, J. A.; Lehnerr, I.; St Louis, V. L.;
282 Heimbürger, L. E.; Sonke, J. E.; Krabbenhoft, D. P.; Sunderland, E. M. A Mass Budget
283 for Mercury and Methylmercury in the Arctic Ocean. *Global Biogeochem. Cycles* **2016**,
284 *30* (4), 560–575. <https://doi.org/10.1002/2015GB005280>.
- 285 (13) Gosselin, M.; Levasseur, M.; Wheeler, P. A.; Horner, R. A.; Booth, B. C. New
286 Measurements of Phytoplankton and Ice Algal Production in the Arctic Ocean. *Deep. Res.*
287 *Part II Top. Stud. Oceanogr.* **1997**, *44* (8), 1623–1644. [https://doi.org/10.1016/S0967-](https://doi.org/10.1016/S0967-0645(97)00054-4)
288 [0645\(97\)00054-4](https://doi.org/10.1016/S0967-0645(97)00054-4).
- 289 (14) Boetius, A.; Albrecht, S.; Bakker, K.; Bienhold, C.; Felden, J.; Fernández-Méndez, M.;
290 Hendricks, S.; Katlein, C.; Lalande, C.; Krumpen, T.; et al. Export of Algal Biomass from

- 291 the Melting Arctic Sea Ice. *Science* (80-.). **2013**, 339 (6126), 1430–1432.
292 <https://doi.org/10.1126/science.1231346>.
- 293 (15) Kwok, R. Arctic Sea Ice Thickness, Volume, and Multiyear Ice Coverage: Losses and
294 Coupled Variability (1958-2018). *Environ. Res. Lett.* **2018**, 13 (10).
295 <https://doi.org/10.1088/1748-9326/aae3ec>.
- 296 (16) Chaulk, A.; Stern, G. A.; Armstrong, D.; Barber, D. G.; Wang, F. Mercury Distribution
297 and Transport across the Ocean- Sea-Ice- Atmosphere Interface in the Arctic Ocean.
298 *Environ. Sci. Technol.* **2011**, 45 (5), 1866–1872.
- 299 (17) Peeken, I.; Primpke, S.; Beyer, B.; Gütermann, J.; Katlein, C.; Krumpfen, T.; Bergmann,
300 M.; Hehemann, L.; Gerdt, G. Arctic Sea Ice Is an Important Temporal Sink and Means of
301 Transport for Microplastic. *Nat. Commun.* **2018**, 9 (1). [https://doi.org/10.1038/s41467-](https://doi.org/10.1038/s41467-018-03825-5)
302 [018-03825-5](https://doi.org/10.1038/s41467-018-03825-5).
- 303 (18) Munson, K. M.; Babi, D.; Lamborg, C. H. Determination of Monomethylmercury from
304 Seawater with Ascorbic Acid-Assisted Direct Ethylation. *Limnol. Oceanogr. Methods*
305 **2014**, 12 (1 JAN), 1–9. <https://doi.org/10.4319/lom.2014.12.1>.
- 306 (19) United States Environmental Protection Agency. *Method 1631, Revision E: Mercury in*
307 *Water by Oxidation, Purge and Trap, and Cold Vapour Atomic Fluorescence*
308 *Spectrometry*; Washington, DC, 2002.
- 309 (20) United States Environmental Protection Agency. *Method 1630: Methylmercury in Water*
310 *by Distillation , Aqueous Ethylation , Purge and Trap, and Cold Vapor Atomic*
311 *Fluorescence*; Washington, DC, 2001.
- 312 (21) Cossa, D.; Durrieu de Madron, X.; Schäfer, J.; Lanceleur, L.; Guédron, S.; Buscaïl, R.;
313 Thomas, B.; Castelle, S.; Naudin, J.-J. The Open Sea as the Main Source of

- 314 Methylmercury in the Water Column of the Gulf of Lions (Northwestern Mediterranean
315 Margin). *Geochim. Cosmochim. Acta* **2017**, *199*, 222–237.
316 <https://doi.org/10.1016/j.gca.2016.11.037>.
- 317 (22) Rosati, G.; Heimbürger, L. E.; Melaku Canu, D.; Lagane, C.; Laffont, L.; Rijkenberg, M.
318 J. A.; Gerringa, L. J. A.; Solidoro, C.; Gencarelli, C. N.; Hedgecock, I. M.; et al. Mercury
319 in the Black Sea: New Insights From Measurements and Numerical Modeling. *Global*
320 *Biogeochem. Cycles* **2018**, *32* (4), 529–550. <https://doi.org/10.1002/2017GB005700>.
- 321 (23) Cox, G. F. N.; Weeks, W. F. Equations for Determining the Gas and Brine Volumes in
322 Sea Ice Samples. *CRREL Rep. (US Army Cold Reg. Res. Eng. Lab.* **1982**, *29* (102), 306–
323 316. <https://doi.org/10.3189/s0022143000008364>.
- 324 (24) Fetterer, F., K. Knowles, W. N. Meier, M. Savoie, and A. K. W. Sea Ice Index, Version 3.
325 NSIDC: National Snow and Ice Data Center. <https://doi.org/10.7265/N5K072F8>.
- 326 (25) Tschudi, M. A.; Stroeve, J. C.; Stewart, J. S. Relating the Age of Arctic Sea Ice to Its
327 Thickness, as Measured during Nasa’s ICESat and IceBridge Campaigns. *Remote Sens.*
328 **2016**, *8* (6). <https://doi.org/10.3390/rs8060457>.
- 329 (26) Bowman, J. S.; Rasmussen, S.; Blom, N.; Deming, J. W.; Rysgaard, S.; Sicheritz-Ponten,
330 T. Microbial Community Structure of Arctic Multiyear Sea Ice and Surface Seawater by
331 454 Sequencing of the 16S RNA Gene. *ISME J.* **2012**, *6* (1), 11–20.
332 <https://doi.org/10.1038/ismej.2011.76>.
- 333 (27) Bowman, J. S. The Relationship between Sea Ice Bacterial Community Structure and
334 Biogeochemistry: A Synthesis of Current Knowledge and Known Unknowns. *Elementa*
335 **2015**, *3*, 1–20. <https://doi.org/10.12952/journal.elementa.000072>.
- 336 (28) Zhou, J.; Delille, B.; Eicken, H.; Vancoppenolle, M.; Brabant, F.; Carnat, G.; Geilfus, N.

- 337 X.; Papakyriakou, T.; Heinesch, B.; Tison, J. L. Physical and Biogeochemical Properties
338 in Landfast Sea Ice (Barrow, Alaska): Insights on Brine and Gas Dynamics across
339 Seasons. *J. Geophys. Res. Ocean.* **2013**, *118* (6), 3172–3189.
340 <https://doi.org/10.1002/jgrc.20232>.
- 341 (29) Moreau, S.; Vancoppenolle, M.; Zhou, J.; Tison, J. L.; Delille, B.; Goosse, H. Modelling
342 Argon Dynamics in First-Year Sea Ice. *Ocean Model.* **2014**, *73*, 1–18.
343 <https://doi.org/10.1016/j.ocemod.2013.10.004>.
- 344 (30) Miller, L. A.; Papakyriakou, T. N.; Collins, R. E.; Deming, J. W.; Ehn, J. K.; MacDonald,
345 R. W.; Mucci, A.; Owens, O.; Raudsepp, M.; Sutherland, N. Carbon Dynamics in Sea Ice:
346 A Winter Flux Time Series. *J. Geophys. Res. Ocean.* **2011**, *116* (2), 6058.
347 <https://doi.org/10.1029/2009JC006058>.
- 348 (31) Agather, A. M.; Hammerschmidt, C. R.; Lamborg, C. H.; Bowman, K. L. Distribution of
349 Mercury Species in the Western Arctic Ocean (U.S. GEOTRACES GN01). **2016**, No.
350 May. <https://doi.org/10.1130/abs/2016nc-275172>.
- 351 (32) Lesins, G.; Duck, T.; Drummond, J. Climate Trends at Eureka in the Canadian High
352 Arctic. *Atmos. - Ocean* **2010**, *48* (2), 59–80. <https://doi.org/10.3137/AO1103.2010>.
- 353 (33) Wanninkhof, R. Relationship between Wind Speed and Gas Exchange over the Ocean
354 Revisited. *J. Geophys. Res.* **1992**, *97* (C5), 7373–7382.
355 <https://doi.org/10.4319/lom.2014.12.351>.
- 356 (34) Liss, P. S.; Merlivat, L. Air-Sea Gas Exchange Rates: Introduction and Synthesis. In *The*
357 *Role of Air-Sea Exchange in Geochemical Cycling*; Springer Netherlands: Dordrecht,
358 1986; pp 113–127. https://doi.org/10.1007/978-94-009-4738-2_5.
- 359 (35) Nightingale, P. D.; Malin, G.; Law, C. S.; Watson, A. J.; Liss, P. S.; Liddicoat, M. I.;

360 Boutin, J.; Upstill-Goddard, R. C. In Situ Evaluation of Air-Sea Gas Exchange
361 Parameterizations Using Novel Conservative and Volatile Tracers. *Global Biogeochem.*
362 *Cycles* **2000**, *14* (1), 373–387. <https://doi.org/10.1029/1999GB900091>.
363 (36) Schartup, A. T.; Qureshi, A.; Dassuncao, C.; Thackray, C. P.; Harding, G.; Sunderland, E.
364 M. A Model for Methylmercury Uptake and Trophic Transfer by Marine Plankton.
365 *Environ. Sci. Technol.* **2018**, *52* (2), 654–662. <https://doi.org/10.1021/acs.est.7b03821>.
366 (37) Post, E.; Bhatt, U. S.; Bitz, C. M.; Brodie, J. F.; Fulton, T. L.; Hebblewhite, M.; Kerby, J.;
367 Kutz, S. J.; Stirling, I.; Walker, D. A. Ecological Consequences of Sea-Ice Decline.
368 *Science* (80-.). **2013**, *341* (August), 519–525. <https://doi.org/10.1126/science.1235225>.
369 (38) Wassmann, P. Arctic Marine Ecosystems in an Era of Rapid Climate Change. *Prog.*
370 *Oceanogr.* **2011**, *90* (1–4), 1–17. <https://doi.org/10.1016/j.pocean.2011.02.002>.
371 (39) Cossa, D.; Martin, J. M.; Sanjuan, J.; Martint, J.; Sanjuan, J. Dimethylmercury Formation
372 in the Alboran Sea. *Mar. Pollut. Bull.* **1994**, *28* (6), 381–384.
373 [https://doi.org/10.1016/0025-326X\(94\)90276-3](https://doi.org/10.1016/0025-326X(94)90276-3).
374
375

376
 377
 378
 379
 380
 381
 382
 383
 384
 385

Table 1: Summary of sea-ice core characteristics and mean speciated mercury (Hg) concentrations (the standard deviation represents downcore variability).

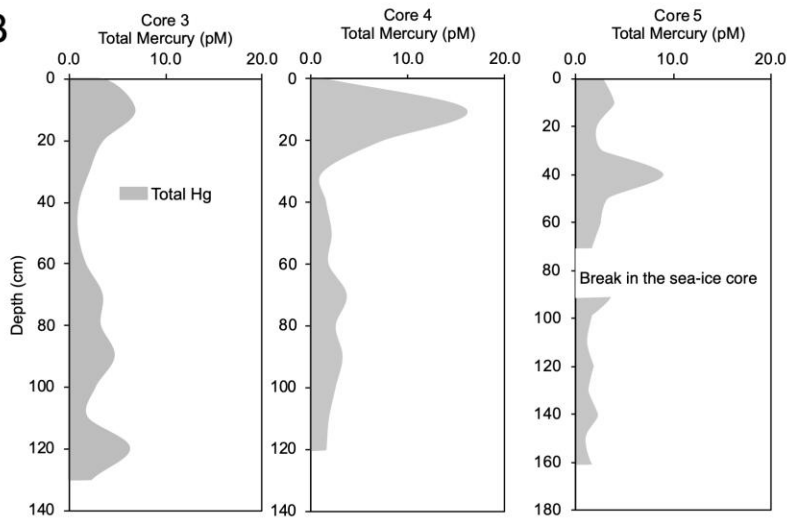
Sea-ice Core	Station	Core thickness cm	Sea-ice Temperature °C	Salinity	Total Hg [†] pM	MeHg [‡] pM	DMHg [‡] pM	MeHg: Total Hg %	DMHg: MeHg %
1	46	85	-1.07	1.31	2.7±3.2	0.120±0.028	--	8.2	--
2	54*	167	-1.57	2.38	2.6±3.1	0.016±0.015	--	1.1	--
3	69	133	-1.73	1.37	3.0±1.9	0.086±0.101	0.048±0.094	3.0	34
4	81	135	-3.40	2.79	3.6±4.6	0.085±0.076	0.027±0.032	2.3	26
5	96*	151	-1.90	3.02	2.6±1.9	0.032±0.017	0.015±0.015	1.0	41
6	101	135	-4.08	3.45	2.5±0.8	0.115±0.043	--	5.0	--

* Multi-year sea-ice cores
[†] The method detection limit is 0.08 pM
[‡] The method detection limit is 0.011 pM

A



B



C

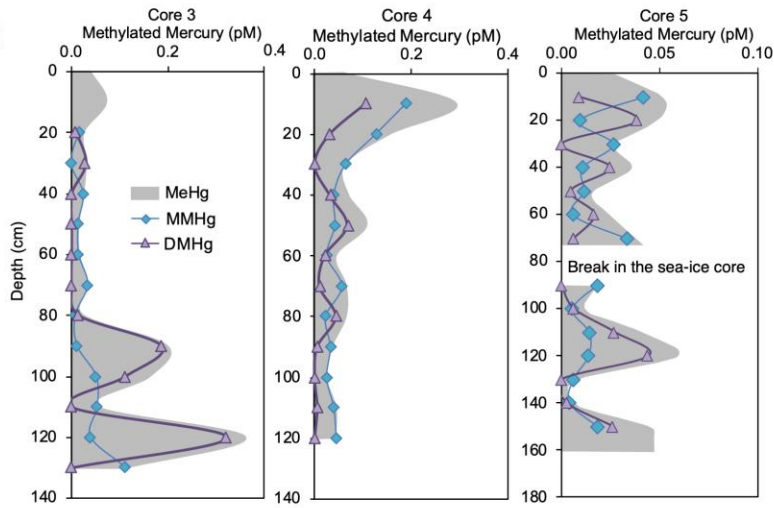
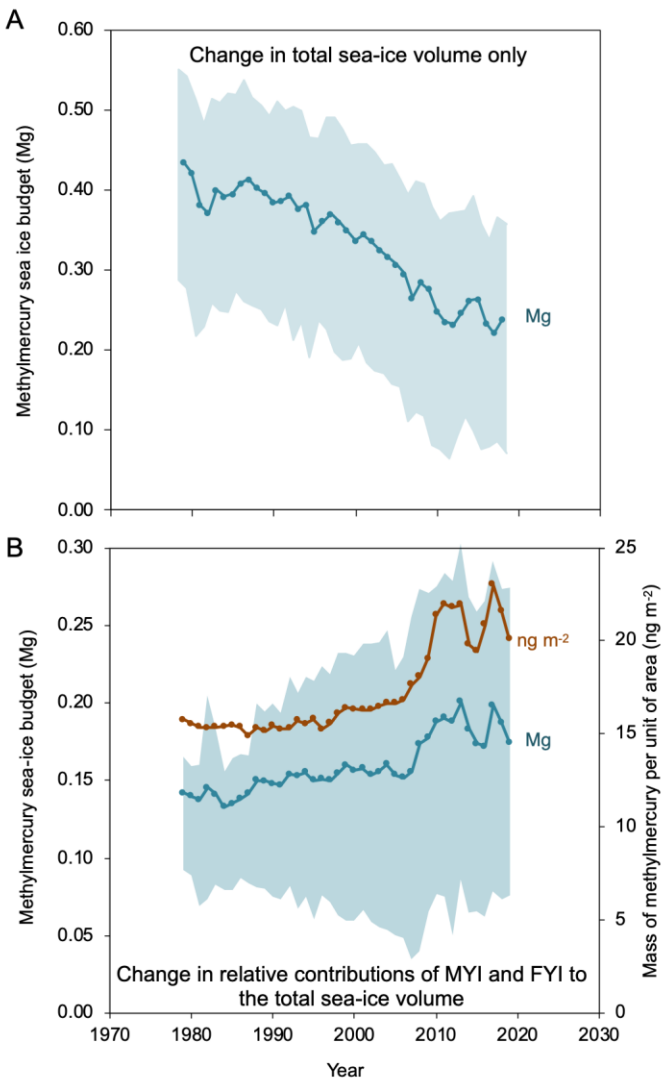


Figure 1

387
388
389



390
391
392

Figure 2